Anisotropic muonium with random hyperfine distortions: A new static relaxation theory

Ralph Eric Turner and Dale R. Harshman*
TRIUMF, 4004 Wesbrook Mall, Vancouver, British Columbia, Canada V6T 2A3
(Received 17 December 1985)

The spin dynamics associated with random hyperfine distortions of an ensemble of muons, which have thermalized in a solid as static muonium atoms, is approximated with the motion generated by averaging the spin evolution of a single isolated anisotropic muonium atom over a product of continuous hyperfine frequency distributions. That is, since each muonium atom in the ensemble is assumed to have a given set of nonunique anisotropic hyperfine frequencies, then the frequency distributions represent the ensemble average of many such muonium atoms. The hyperfine tensor includes an isotropic Fermi contact term and a symmetric traceless dipole-dipole term. There is no antisymmetric contribution. In this work the hyperfine tensor is expanded in terms of second-rank spherical tensors while the expansion coefficients are used to parametrize the distortion. Thus there are six frequencies associated with an anisotropic muonium atom, one associated with the isotropic part of the hyperfine tensor and five corresponding to the anisotropic components. Relaxation functions are calculated for muonium in both the zero- and high-field limits. The different anisotropic components of the hyperfine tensor lead to different (anisotropic) observable motion functions. For an amorphous or powder sample, only the isotropic motion function is observable, and the different anisotropic frequencies lead to motion functions with differing shapes. These functions have been applied to the case of fused quartz where the spin relaxation is well known to be entirely due to random hyperfine distortions.

I. INTRODUCTION

Muon-spin-rotation (μSR) experiments[1-5] in condensed matter begin with the thermalization of spin polarized positive muons in chemical species whose muon magnetic state is either diamagnetic or paramagnetic. The dynamics of the spin polarization of an ensemble of such muons is observed via the asymmetric decay of the muon; the positron is emitted preferentially along the muon's spin vector. Commonly, a "time-differential" technique is used in which a clock is started on an incident muon and stopped upon the detection of a positron. This information is then used to construct a time histogram which has the form

$$N_0 \exp(-t/\tau_\mu)[1+A_0 S(t)]+B_0 ,$$

where $\tau_\mu \approx 2.2$ μs is the muon's lifetime, N_0 is a normalization constant, A_0 is the initial signal amplitude, B_0 is a background constant, and $S(t)$ is the unit normalized signal. In zero-field and longitudinal-field experiments this signal is a relaxation function and is usually denoted as $G(t)$. On the other hand, in transverse-field experiments the signal $S(t)$ is the product of a relaxation function and oscillatory terms. For consistency the symbol $G(t)$ will be used to denote the signals for both cases in this work and it will be termed a motion function. These motion functions are coefficients of the second-rank dynamical motion tensor which generates the dynamics of the muon's spin vector. This second-rank motion tensor is simply the spin-vector–spin-vector autocorrelation tensor for the muon.

For a static muonium atom in a solid the Hamiltonian involves operators for the spin degree of freedom for both the muon and the electron, all degrees of freedom of the solid and all interactions between the solid and the muonium atom. The spin Hamiltonian of the muonium atom involves the Zeeman terms associated with the applied field and the general anisotropic hyperfine tensor which couples the electron spin to the muon spin. There are five known relaxation mechanisms by which the muon spin may depolarize, that is, by interactions with random local magnetic fields, by chemical reactions, by spin exchange, by superhyperfine interactions, and by random anisotropic hyperfine distortions. Relaxation functions for the first four have been treated in the literature, while they have not been developed for the latter. This paper addresses itself to the solution of this problem. In particular the spin polarization is determined by the induced distortion in the electron wave function of each muonium atom. Although interactions of this type do not lead to a relaxation of the muon spin polarization for the individual muonium atoms, depolarization can occur via ensemble dephasing provided that there is a random distribution in the distortion parameters of the individual muonium atoms in the ensemble. A full quantal calculation of the dynamics of the spin vector of the muon for such a situation is very complicated. Rather than performing such a numerical calculation an ensemble random hyperfine approximation is adopted. That is, the interaction of the individual static muonium atoms with the solid is assumed to be completely described by a general anisotropic hyperfine tensor with given nonunique hyperfine frequencies. On the other hand, the ensemble average over many such muonium atoms is approximated by a product of averages over continuous frequency distributions of the motion of a single muonium atom.

 ©1986 The American Physical Society

There are two frames of reference to be considered, namely, the lab frame and the crystal frame. The former is defined by the physical geometry of the counters which are arranged normal to the directions of an orthonormal coordinate system labeled X,Y,Z. If an external magnetic field $\mathbf{B}$ is applied, then by definition its direction is taken to be $\hat{\mathbf{Z}}$. In this coordinate system the incoming muon's momentum is assumed to lie in the $\hat{\mathbf{X}}$ direction while its spin vector,

$$I_{\rm in}[\hat{\mathbf{Z}}\cos\theta_{\rm in}+\sin\theta_{\rm in}(\hat{\mathbf{X}}\cos\phi_{\rm in}+\hat{\mathbf{Y}}\sin\phi_{\rm in})] ,$$

defines the skew angles $\theta_{\rm in}$ and $\phi_{\rm in}$. The crystal frame, defined by the orthonormal coordinates x,y,z, is related to the counter frame by the three Euler angles, $\omega'=\alpha,\beta,\gamma$, through the rotation tensor

$$\vec{\vec{\mathbf{R}}}(\omega')=\exp(-i\vec{\vec{\mathbf{J}}}_z\alpha)\cdot\exp(-i\vec{\vec{\mathbf{J}}}_y\beta)\cdot\exp(-i\vec{\vec{\mathbf{J}}}_z\gamma) ,$$

that is, for example, $\hat{\mathbf{x}}=\vec{\vec{\mathbf{R}}}(\omega')\cdot\hat{\mathbf{X}}$. Here, $\vec{\vec{\mathbf{J}}}_A=-i\vec{\vec{\epsilon}}^{(3)}\cdot\hat{\mathbf{A}}$ is the infinitesimal rotation tensor while $\vec{\vec{\epsilon}}^{(3)}$ is the Levi-Cevita[6] third-rank antisymmetric tensor. On the other hand, this relation can be inverted, that is, $\hat{\mathbf{X}}=\vec{\vec{\mathbf{R}}}(\Omega')\cdot\hat{\mathbf{x}}$, where $\Omega'=-\gamma,-\beta,-\alpha$ are the inverse Euler angles. Observations are performed in the counterframe, whereas, especially for zero-field experiments, the motion is more readily described in terms of the crystal frame.

Expressions for the observable longitudinal, coplanar transverse, and perpendicular transverse motion functions, which involve both counter and crystal frame motion functions, are reviewed in Sec. II. The continuous ensemble approximation for the random anisotropic hyperfine interaction is defined in Sec. III while, in Sec. IV, the motion functions are expressed in terms of the motion tensors associated with isolated anisotropic muonium atoms. In the latter the eigenvectors of isolated isotropic muonium atoms are used as basis functions. In Sec. V zero-field motion functions associated with two simple examples are considered, namely, anisotropic hyperfine tensors with (i) nonzero ω_{20} and (ii) nonzero $\omega_{20},\omega_{2\pm2}$ while, in Sec. VI, large applied external field motion functions are considered for the general anisotropic hyperfine tensor. Finally, in Sec. VII, these motion functions are used to fit low-temperature fused-quartz data.

II. OBSERVABLE RELAXATION FUNCTION

For a muonium atom, the expectation value of the muon's dimensionless spin vector $\mathbf{I}$,

$$\begin{aligned}&\langle\mathbf{I}\rangle(t)=\mathrm{Tr}\mathbf{I}(t)[1_\mu/4+\mathbf{I}\cdot\mathbf{I}_{\rm in}]1_e\rho_s(0)=\vec{\vec{\mathbf{G}}}(t)\cdot\mathbf{I}_{\rm in} ,\\ &\vec{\vec{\mathbf{G}}}(t)=\mathrm{Tr}\exp(iHt/\hbar)\mathbf{I}\exp(-iHt/\hbar)\mathbf{I}\rho_s(0) ,\end{aligned} \tag{2.1}$$

has motion generated by the corresponding muon dynamical motion tensor $\vec{\vec{\mathbf{G}}}(t)$, which is the muon-spin-vector time autocorrelation tensor. This expectation value involves the Hamiltonian H for the muonium-environment system and the initial spin-density operators for muonium, $[1_\mu/4+\mathbf{I}\cdot\mathbf{I}_{\rm in}]1_e$, and for the solid, $\rho_s(0)$. It can be written in terms of nine observable motion functions which are related to the nine coefficients of the counterframe spherical tensor resolution of $\vec{\vec{\mathbf{G}}}(t)$. In particular, the muon's spin expectation value,

$$\begin{aligned}&\langle\mathbf{I}\rangle(t)=I_{\rm in}[G_{\rm L}(t)\hat{\mathbf{Z}}+G_{\rm PT}(t)\hat{\mathbf{X}}+G_{\rm CT}(t)\hat{\mathbf{Y}}] ,\\ &G_A(t)=\cos\theta_{\rm in}G_A^C(t)+\sin\theta_{\rm in}[\cos\phi_{\rm in}G_A^{SC}(t)\\ &\qquad\qquad+(\sin\phi_{\rm in})G_A^{SS}(t)] ,\end{aligned} \tag{2.2}$$

involves three observable longitudinal (L) motion functions,

$$\begin{aligned}&G_{\rm L}^C(t)=G_{00}(t)-(\tfrac{2}{3})^{1/2}G_{20}(t) ,\\ &G_{\rm L}^{SC}(t)=\mathrm{Im}G_{11}(t)+\mathrm{Re}G_{21}(t) ,\\ &G_{\rm L}^{SS}(t)=-\mathrm{Re}G_{11}(t)+\mathrm{Im}G_{21}(t) ,\end{aligned} \tag{2.3}$$

three coplanar transverse (CT) motion functions,

$$\begin{aligned}&G_{\rm CT}^C(t)=-\mathrm{Im}G_{11}(t)+\mathrm{Re}G_{21}(t) ,\\ &G_{\rm CT}^{SC}(t)=G_{00}(t)+\tfrac{1}{2}(\tfrac{2}{3})^{1/2}G_{20}(t)-\mathrm{Re}G_{22}(t) ,\\ &G_{\rm CT}^{SS}(t)=-(2)^{-1/2}G_{10}(t)-\mathrm{Im}G_{22}(t) ,\end{aligned} \tag{2.4}$$

and three perpendicular transverse (PT) motion functions,

$$\begin{aligned}&G_{\rm PT}^C(t)=\mathrm{Re}G_{11}(t)+\mathrm{Im}G_{21}(t) ,\\ &G_{\rm PT}^{SC}(t)=(2)^{-1/2}G_{10}(t)-\mathrm{Im}G_{22}(t) ,\\ &G_{\rm PT}^{SS}(t)=G_{00}(t)+\tfrac{1}{2}(\tfrac{2}{3})^{1/2}G_{20}(t)+\mathrm{Re}G_{22}(t) .\end{aligned} \tag{2.5}$$

The standard longitudinal motion function is $G_{\rm L}^C(t)$, while the standard transverse-field motion functions are either $G_{\rm CT}^{SC}(t)$ or $G_{\rm PT}^{SS}(t)$. On the other hand, all nine motion functions can, in principle, be observed[7,8] if the skew angle $\theta_{\rm in}$ is assumed to be fixed such that $\sin\theta_{\rm in}\neq\cos\theta_{\rm in}\neq0$ and if three values of the skew angle $\phi_{\rm in}$ are used. If this is accomplished through the use of a spin rotator[9,10] (a Wein-field filter designed to rotate the muon spin to the desired orientation), then the apparatus does not need to be altered to obtain all nine motion functions. These observable motion functions contain the isotropic, antisymmetric, and symmetric traceless expansion coefficients of the counterframe spherical tensor resolution of the motion tensors, that is,

$$\begin{aligned}&\vec{\vec{\mathbf{G}}}(t)=G_{00}(t)\vec{\vec{\mathbf{U}}}-(i/2^{1/2})\vec{\vec{\epsilon}}^{(3)}\cdot\mathbf{E}_M^1G_{1M}(t)+\vec{\mathbf{E}}_M^2G_{2M}(t) ,\\ &G_{00}(t)=\tfrac{1}{3}\vec{\vec{\mathbf{U}}}:\mathbf{G}(t),\quad G_{1M}(t)=(-i/2^{1/2})\mathbf{E}^{1M}\cdot\vec{\vec{\epsilon}}^{(3)}:\vec{\vec{\mathbf{G}}}(t) ,\\ &G_{2M}(t)=\vec{\mathbf{E}}^{2M}:\vec{\vec{\mathbf{G}}}(t),\quad G_{L-M}(t)=(-1)^MG_{LM}(t)^* .\end{aligned} \tag{2.6}$$

The summation convention for repeated indices is assumed throughout. Here $\vec{\vec{\mathbf{U}}}$ is the unit second-rank tensor, $\vec{\vec{\epsilon}}^{(3)}\cdot\mathbf{E}_M^1$ are the antisymmetric second-rank tensors constructed from the Levi-Cevita tensor and the counter frame spherical vectors $\mathbf{E}_M^1$, and $\vec{\mathbf{E}}_M^2$ are the second-rank symmetric traceless counter frame spherical tensors. These spherical vectors and tensors and their contravariant counterparts, $\vec{\mathbf{E}}^{LM}=(\vec{\mathbf{E}}_M^L)^*$, are[6,11]

$$\begin{aligned}
&\mathbf{E}^1_{\pm1}=\pm(i/2^{1/2})(\hat{\mathbf{X}}\mp i\hat{\mathbf{Y}}),\ \ \mathbf{E}^1_0=-i\hat{\mathbf{Z}}\ ,\\
&\overleftrightarrow{\mathbf{E}}{}^2_0=(\tfrac{2}{3})^{1/2}[-\hat{\mathbf{Z}}\hat{\mathbf{Z}}+\tfrac{1}{2}(\hat{\mathbf{X}}\hat{\mathbf{X}}+\hat{\mathbf{Y}}\hat{\mathbf{Y}})]\ ,\\
&\overleftrightarrow{\mathbf{E}}{}^2_{\pm1}=\pm\tfrac{1}{2}[(\hat{\mathbf{X}}\hat{\mathbf{Z}}+\hat{\mathbf{Z}}\hat{\mathbf{X}})\mp i(\hat{\mathbf{Z}}\hat{\mathbf{Y}}+\hat{\mathbf{Y}}\hat{\mathbf{Z}})]\ ,\\
&\overleftrightarrow{\mathbf{E}}{}^2_{\pm2}=-\tfrac{1}{2}[(\hat{\mathbf{X}}\hat{\mathbf{X}}-\hat{\mathbf{Y}}\hat{\mathbf{Y}})\mp i(\hat{\mathbf{X}}\hat{\mathbf{Y}}+\hat{\mathbf{Y}}\hat{\mathbf{X}})]\ .
\end{aligned}\tag{2.7}$$

While these observable motion functions have been expressed in terms of the counterframe motion functions they may also be expressed in terms of the crystal-frame motion functions, $g_{Lm}(t)$, through the rotation transformation,

$$G_{LM}(t)=g_{Lm}(t)R^{(L)}_{mM}(\Omega')\ . \tag{2.8}$$

In this way expressions similar to those in Eq. (2.6) are obtained, except using the crystal frame spherical tensors. Equation (2.8) is derived using the relation,[12]

$$\overleftrightarrow{\mathbf{e}}{}^L_m\odot^L\overleftrightarrow{\mathbf{E}}{}^{LM}=\langle Lm\mid R^{(L)}_{op}(\Omega')\mid LM\rangle=R^{(L)}_{mM}(\Omega')\ , \tag{2.9}$$

between the counter- and crystal-frame spherical tensors. This relation involves the matrix elements of the quantal rotation operation.[13]

III. RANDOM HYPERFINE DISTORTIONS

In an applied magnetic field $\mathbf{B}$ the spin Hamiltonian for an isolated anisotropic muonium atom, $H_{\mathrm{Mu}}=\hbar(\gamma_e\mathbf{S}-\gamma_\mu\mathbf{I})\cdot\mathbf{B}+\hbar\overleftrightarrow{\mathbf{W}}:\mathbf{SI}$, involves the Zeeman interactions and the hyperfine tensor. The former contains the dimensionless spin operators for the muon $\mathbf{I}$ and the electrons $\mathbf{S}$, and their gyromagnetic ratios $\gamma_\mu=2\pi\times0.0136$ MHz/G and $\gamma_e=2\pi\times2.80$ MHz/G, respectively, while the latter,

$$\begin{aligned}
&\overleftrightarrow{\mathbf{W}}=\omega_{00}\overleftrightarrow{\mathbf{U}}+\overleftrightarrow{\mathbf{e}}{}^2_M a_{2M}\omega_{2M}=W_{00}\overleftrightarrow{\mathbf{U}}+\overleftrightarrow{\mathbf{E}}{}^2_M a_{2M}W_{2M}\ ,\\
&W_{2M}=R^{(2)}_{Mm}(\Omega')\omega_{2m}\ ,
\end{aligned}\tag{3.1}$$

has coefficients which are defined in the crystal frame. The constants, $a_{20}=(\frac{3}{2})^{1/2}$, $a_{2\pm1}=2^{-3/2}$ and $a_{2\pm2}=\frac{1}{2}$, are chosen to minimize the number of numerical constants involved in the isotropic eigenvector matrix representation of the anisotropic terms. This hyperfine tensor may be derived,[14] in first-order perturbation theory, from the magnetic interaction $\mathbf{B}(\mathbf{r})$ between the electron and the muon, that is,

$$\begin{aligned}
&H_{\mathrm{hyp}}=\hbar\overleftrightarrow{\mathbf{W}}:\mathbf{SI}=\hbar\gamma_e\mathbf{S}\cdot\langle\mathbf{B}(\mathbf{r})\rangle\\
&\qquad=\hbar\gamma_e\mathbf{S}\cdot\int d\mathbf{r}\,\psi(r)^*\mathbf{B}(\mathbf{r})\psi(\mathbf{r})\ ,\\
&\mathbf{B}(\mathbf{r})=-\nabla\times(\mathbf{I}\times\nabla)(\hbar\gamma_\mu/r)\\
&\qquad=\hbar\gamma_\mu\mathbf{I}\cdot\{4\pi\overleftrightarrow{\mathbf{U}}\delta(\mathbf{r})+(3/r^3)[\hat{\mathbf{r}}]^{(2)}\}\ ,\\
&\omega_{00}=(4\pi\hbar\gamma_\mu\gamma_e/3)\langle\delta(\mathbf{r})\rangle\ ,\\
&a_{2M}\omega_{2M}=-[3\hbar\gamma_e\gamma_\mu(8\pi/15)^{1/2}]\langle r^{-3}Y_{2M}(\hat{\mathbf{r}})\rangle\ .
\end{aligned}\tag{3.2}$$

It has no antisymmetric contributions since the magnetic interaction between the electron and the muon has no antisymmetric components. Equation (3.2) involves the symmetric traceless second-rank tensor, $[\hat{\mathbf{r}}]^{(2)}=\hat{\mathbf{r}}\hat{\mathbf{r}}-\overleftrightarrow{\mathbf{U}}/3$, associated with $\hat{\mathbf{r}}$ while the counterframe coefficients of this tensor are simply linear combinations of the crystal-frame coefficients with the rotation matrices acting as the expansion coefficients. The Hamiltonian for the total system is then the sum of this muonium spin Hamiltonian and the Hamiltonian for its interactions with the solid. All such interactions are assumed in this work to only lead to distortions of the electronic wave function of each muonium atom with an associated nonunique anisotropic hyperfine tensor. That is, the electronic states of the muonium atoms, which, for example, may be described by linear combinations of atomic hydrogen orbitals, contain contributions from, at least, the $2s$ and $2p$ states. Indeed, whatever the electronic configuration is, there are at most six coefficients associated with the hyperfine tensor. Such distortions do not lead to relaxation of the muon spin vector for the individual atoms. However, the ensemble of muonium atoms relaxes by ensemble dephasing since each muonium atom in the ensemble has an independent set of hyperfine frequencies. A simple continuous random hyperfine approximation is adopted here to describe this ensemble relaxation. That is, the total Hamiltonian is replaced by the spin Hamiltonian for an isolated muonium atom while the ensemble average (trace over the ensemble density operator) is replaced by a product of integrals,

$$\mathrm{Tr}\rho_S(0)\approx\sum_{LM}\int_{-\infty}^{\infty}d\omega_{LM}F_{LM}(\omega_{LM})\ , \tag{3.3}$$

over a set of random continuous distributions associated with each frequency in the muonium hyperfine tensor. Thus the spin-spin autocorrelation tensor for the muonium ensemble,

$$\begin{aligned}
&[\overleftrightarrow{\mathbf{G}}(t)]^{\mathrm{RH}}=\prod_{L,M}\int_{-\infty}^{\infty}d\omega_{LM}F_{LM}(\omega_{LM})[\overleftrightarrow{\mathbf{G}}(t)]^{\mathrm{Mu}}\ ,\\
&[\overleftrightarrow{\mathbf{G}}(t)]^{\mathrm{Mu}}=\mathrm{Tr}[\mathbf{I}(t)\mathbf{I}]\ ,
\end{aligned}\tag{3.4}$$

is the average over the product of the random hyperfine (RH) distributions of the muon motion tensor whose dynamics is generated by the muonium spin Hamiltonian. Equation (3.4) constitutes the random hyperfine distortion model for the observable muon-spin-motion functions.

IV. ANISOTROPIC MUONIUM AUTOCORRELATION TENSOR

The evaluation of the random hyperfine motion tensor requires expressions for the spin-spin autocorrelation tensor associated with the muonium-atom spin Hamiltonian, H_{Mu}. To solve this problem it is convenient to expand the eigenfunctions of the general muonium atom in terms of the eigenfunctions of the isotropic hyperfine Hamiltonian since, in general, the isotropic hyperfine frequency is much larger than the anisotropic frequencies. In particular, the eigenfunctions of the isotropic Hamiltonian are

$$\begin{aligned}
&|1\rangle_0=|\alpha\alpha\rangle,\ |2\rangle_0=|\beta\beta\rangle\ ,\\
&|3\rangle_0=|\alpha\beta\rangle\sin(\lambda/2)+|\beta\alpha\rangle\cos(\lambda/2)\ ,
\end{aligned}$$

and

$$|4\rangle_0 = |\alpha\beta\rangle \cos(\lambda/2) - |\beta\alpha\rangle \sin(\lambda/2) ,$$

with eigenenergies,

$$E_1 = (\omega_{00} + 4\omega_{Mu})\hbar/4 ,$$

$$E_2 = (\omega_{00} - 4\omega_{Mu})\hbar/4 ,$$

$$E_3 = [\omega_{00} + 4\Omega]\hbar/4 ,$$

and

$$E_4 = -[3\omega_{00} + 4\Omega]\hbar/4 ,$$

respectively. These eigenfunctions and eigenenergies involve the muonium gyromagnetic ratio, $\gamma_{Mu} = \frac{1}{2}(\gamma_e - \gamma_\mu)$, the muonium Larmor frequency, $\omega_{Mu} = \gamma_{Mu} B$, the beat frequency, $\Omega = \frac{1}{2}\omega_{00}[(1+x^2)^{1/2} - 1]$, and the angle $\lambda = \arcsin[1/(1+x^2)^{1/2}]$. This beat frequency and angle involve a parameter $x = B/B_h$ which is the ratio of the field strength B to the hyperfine field $B_h = \omega_{00}/(\gamma_e + \gamma_\mu)$ (= 1585 G in the ground electronic state). The quantization axis is the direction of the field $\mathbf{B}(Z)$ while, by definition, $|\alpha\beta\rangle = |\alpha_\mu \beta_e\rangle$. It is standard terminology in μSR to refer to the states $|1\rangle_0$, $|2\rangle_0$, and $|3\rangle_0$ as triplet muonium and the state $|4\rangle_0$ as singlet muonium. This, of course, is correct terminology for zero field only since these states are not eigenfunctions of the total spin, $\mathbf{F} = \mathbf{S} + \mathbf{I}$, for applied fields. As well, the labels of the second and third eigenfunctions have been interchanged with respect to the standard terminology.

These isotropic eigenfunctions may be used as basis functions for the expansion of the general eigenfunctions,

$$|\psi_i\rangle = c_{ik} |k\rangle_0 \ (E_i = \hbar w_i/4) ,$$

of H_{Mu}. Explicit expressions for the motion functions, Eqs. (2.2)–(2.6), are given in Appendix A. On the other hand, the matrix representation of the hyperfine Hamiltonian involves four matrices, three of which are block diagonal, that is

$$H_{00} = (\hbar/4) \begin{pmatrix} (\omega_{00}+4\omega_{Mu}) & 0 & 0 & 0 \\ 0 & (\omega_{00}-4\omega_{Mu}) & 0 & 0 \\ 0 & 0 & (\omega_{00}+4\Omega) & 0 \\ 0 & 0 & 0 & -(+3\omega_{00}+4\Omega) \end{pmatrix} ,$$

$$H_{20} = (\hbar/4)(W_{20}) \begin{pmatrix} -1 & 0 & 0 & 0 \\ 0 & -1 & 0 & 0 \\ 0 & 0 & 2C^2 & 2SC \\ 0 & 0 & 2SC & 2S^2 \end{pmatrix} , \tag{4.1}$$

$$H_{22} = H^{\dagger}_{2-2} = (\hbar/4) \begin{pmatrix} 0 & -W^*_{22} & 0 & 0 \\ -W_{22} & 0 & 0 & 0 \\ 0 & 0 & 0 & 0 \\ 0 & 0 & 0 & 0 \end{pmatrix} .$$

These matrices, which correspond to the even m components of the spherical tensor expansion of the hyperfine tensor, involve the sine, $S = \sin(\frac{1}{2}\theta)$, and cosine, $C = \cos(\frac{1}{2}\theta)$, of the angle $\theta = \frac{1}{2}\pi - \lambda$, while the matrix associated with the odd m components couple the two blocks, that is

$$H_{21} = H^{\dagger}_{2-1} = (\hbar/4) \begin{pmatrix} 0 & 0 & CW^*_{21} & SW^*_{21} \\ 0 & 0 & -CW_{21} & -SW_{21} \\ CW_{21} & -CW^*_{21} & 0 & 0 \\ SW_{21} & -SW^*_{21} & 0 & 0 \end{pmatrix} . \tag{4.2}$$

The evaluation of the random hyperfine relaxation functions for a single crystal then involve the evaluation of the counterframe hyperfine frequencies obtained from the product of the rotation matrices and the given crystal-frame hyperfine frequencies. This is followed by the evaluation of the eigenfunctions of H_{Mu} using Eqs. (4.1) and (4.2). Their coefficients in this isotropic hyperfine basis are then used to obtain the observable relaxation functions, Eqs. (A2)–(A4), which are then averaged over with the random hyperfine frequency distributions.

For zero-field experiments the angle θ becomes zero and the hyperfine tensor reduces to the following when the axis of quantization is taken as the crystal-frame axis z,

$$H_{\mathrm{Mu}}=(\hbar/4)\begin{bmatrix}(\omega_{00}-\omega_{20}) & -\omega_{22}^{*} & \omega_{21}^{*} & 0\\ -\omega_{22} & (\omega_{00}-\omega_{20}) & -\omega_{21} & 0\\ \omega_{21} & -\omega_{21}^{*} & (\omega_{00}+2\omega_{20}) & 0\\ 0 & 0 & 0 & -3\omega_{00}\end{bmatrix} . \tag{4.3}$$

Since the symmetric traceless components of the hyperfine tensor do not couple to the singlet state, then it is an eigenfunction in zero field. As well the only dependence on the Euler angles occurs through the relation, Eq. (2.8), between the counter- and crystal-frame relaxation, functions. The frequencies are independent of the orientation.

V. ZERO-FIELD RELAXATION FUNCTIONS

To illustrate this random hyperfine approximation for zero-applied-field experiments two specific types of anisotropic muonium atoms are considered, that is, (i) those with nonzero ω_{20} and (ii) those with nonzero $\omega_{20},\omega_{2\pm2}$. These forms of anisotropic hyperfine tensors are chosen because, in certain situations, their motion can be solved analytically. As well, the motion functions can be written in terms of a "triplet" signal, which is independent of the average isotropic hyperfine frequency, and a "singlet" signal which involves the cosine and, possibly, the sine of the product of the isotropic hyperfine frequency and the time. These signals are so named because, in zero fields and with no anisotropic hyperfine frequencies, the triplet signal is that from transitions between two true triplet states, while the singlet signal arises from transitions between a true triplet state and the true singlet state. While in applied fields and with anisotropic hyperfine tensors the states are no longer triplets and singlets, this nomenclature provides a simple way of distinguishing the various signals.

A. Cylindrical anisotropy

Muonium atoms with cylindrical symmetry about some given axis have nonzero ω_{20} as well as nonzero ω_{00}. In general, there may be more than one orientation of this cylindrical axis with respect to the given crystal frame (x,y,z). If all the sites have identical symmetry axes (z) then the resulting zero-field motion can be easily computed. In particular, the crystal-frame Hamiltonian is diagonal for this situation; see Eq. (4.3). Thus its eigenfunctions are the isotropic eigenfunctions and its eigenenergies are the diagonal elements. There are, of course, sixteen frequencies associated with this 4×4 Hamiltonian matrix, four of which are trivially zero. The remaining twelve appear in two groups of six with equal magnitudes but opposite signs. For the present Hamiltonian there is a single (zero) triplet frequency $w_{12}=0$ and a pair of degenerate triplet frequencies $w_{13}=w_{23}=-3\omega_{20}/4$. The singlet frequencies have the same symmetry; that is, there is a single (nonzero) singlet frequency $w_{34}=\omega_{00}+\omega_{20}/2$ and a pair of degenerate frequencies, $w_{24}=\omega_{14}=\omega_{00}-\omega_{20}/4$. Thus, the nonzero crystal-frame motion functions associated with this Hamiltonian are of the form

$$\begin{aligned} g_{00}(t)&=6^{-1}\sum_{\substack{i,j\\ i<j}}\cos(w_{ij}t)\ ,\\ g_{20}(t)&=6^{-1/2}[\tfrac{1}{2}\cos(w_{13}t)+\tfrac{1}{2}\cos(w_{23}t)-\cos(w_{12}t)]\\ &\quad+6^{-1/2}[\tfrac{1}{2}\cos(w_{14}t)+\tfrac{1}{2}\cos(w_{24}t)-\cos(w_{34}t)]\ , \end{aligned} \tag{5.1}$$

where the explicit values of the frequencies are given above. Random hyperfine motion functions are obtained from these single muonium-atom motion functions by averaging over the frequency distributions, Eq. (3.4). To illustrate this procedure Gaussian distributions with nonzero average frequencies, $\bar{\omega}_{LM}$, are assumed, that is,

$$F_{LM}(\omega_{LM})=(2\pi\sigma_{LM}^{2})^{-1/2}\times\exp[-(\omega_{LM}-\bar{\omega}_{LM})^{2}/2\sigma_{LM}^{2}]\ . \tag{5.2}$$

It is also useful to define the dimensionless frequency distributions, $f_{LM}(z)=\exp(-z^{2})$. Thus, for example, the random hyperfine isotropic motion function associated with the Gaussian distribution is the following:

$$\begin{aligned} g_{00}(t)&=6^{-1}[1+2\cos(\bar{w}_{13}t)h_{20}(3t/4)]+6^{-1}[\cos(\bar{w}_{34}t)h_{00}(t)h_{20}(\tfrac{1}{2}t)+2\cos(\bar{w}_{14}t)h_{00}(t)h_{20}(t/4)]\ ,\\ h_{LM}(t)&=\int_{0}^{\infty}dz\,f_{LM}(z)\cos[2^{1/2}\sigma_{LM}tz]=\exp(-t_{LM}^{2}/4)\ , \end{aligned} \tag{5.3}$$

where the dimensionless time is $t_{LM}=2^{1/2}\sigma_{LM}t$ and where $\bar{w}_{ij}$ is the appropriate eigenfrequency evaluated with the average hyperfine frequencies, $\bar{\omega}_{LM}$. The functions $h_{LM}(t)$ are relaxation functions. If the sample of interest is a powder or amorphous then all the Euler angles must be averaged over with equal weights. Thus the only nonzero observable motion functions, $G_{L}^{C}(t)$, $G_{CT}^{SC}(t)$, and $G_{PT}^{SS}(t)$, are all given by the isotropic crystal frame motion functions, Eq. (5.3). The singlet motion functions decay to zero for long times while the triplet motion functions have long-time tails of one sixth (one third of the initial triplet muonium polarization). This long-time tail, which occurs because there is a nontrivial zero-frequency component of the triplet motion, is a distinctive trademark of cylindrical anisotropy. It is lost when

other anisotropic components are included as the doubly degenerate eigenenergies are split, that is, when there is no longer a nontrivial zero frequency. Thus, when an experiment is performed using powders, the long-time behavior immediately demonstrates the lack of, or presence of, anisotropies other than the cylindrical one.

The cylindrical random hyperfine crystal-frame motion functions,

$$g_{20}(t)=6^{-1/2}[\cos(\bar{w}_{13}t)h_{20}(t)-1]+6^{-1/2}[\cos(\bar{w}_{14}t)h_{00}(t/4)-\cos(\bar{w}_{34}t)h_{00}(t)h_{20}(\tfrac{1}{2}t)] , \tag{5.4}$$

are observable if experiments are performed on single crystals. In particular, if the crystal and counter frames are synonymous, $\Omega_1'=0$, the nonzero observable random hyperfine motion functions are

$$\begin{aligned} &G_{\mathrm{L}}^{C}(t \mid \Omega_1')=\tfrac{1}{2}[1+\cos(\bar{w}_{34}t)h_{00}(t)h_{20}(\tfrac{1}{2}t)] , \\ &G_{\mathrm{CT}}^{SC}(t \mid \Omega_1')=G_{\mathrm{PT}}^{SS}(t \mid \Omega_1')=\tfrac{1}{2}\cos(\bar{w}_{13}t)h_{20}(3t/4)+\tfrac{1}{2}\cos(\bar{w}_{14}t)h_{00}(t)h_{20}(t/4) . \end{aligned} \tag{5.5}$$

The two transverse motion functions, which are equal, decay to zero for long times while the longitudinal motion function has a one half time tail. In contrast, for $\Omega_2'=0, -\pi/2, 0$, the observable longitudinal and perpendicular transverse motion functions are the same as the transverse Ω_1' motion functions while the coplanar transverse motion function becomes the same as the Ω_1' longitudinal motion function.

B. Planar plus cylindrical anisotropies

Muonium atoms with $L=2$, $M=0,2,-2$ anisotropies are now considered. Again all the sites are assumed to have identical crystal axes. The crystal-frame Hamiltonian, Eq. (4.3), is block diagonal for this combination of anisotropies and has eigenfunctions and eigenenergies of the form

$$\begin{aligned} &|\phi_1\rangle=2^{-1/2}[\,|1\rangle_0+\exp(i\phi_{22})\,|2\rangle_0], \quad E_1=(\hbar/4)(\omega_{00}-\omega_{20}+\omega_{22}^{M}) , \\ &|\phi_2\rangle=2^{-1/2}[\,|1\rangle_0-\exp(i\phi_{22})\,|2\rangle_0], \quad E_2=(\hbar/4)(\omega_{00}-\omega_{20}-\omega_{22}^{M}) , \\ &|\phi_3\rangle=|3\rangle_0, E_3=(\hbar/4)(\omega_{00}+2\omega_{20}), \quad |\phi_4\rangle=|4\rangle_0, \quad E_4=(\hbar/4)(-3\omega_{00}) , \end{aligned} \tag{5.6}$$

wherein the frequencies ω_{22} and $\omega_{2\,-2}$ are written as $\omega_{22}^{M}\exp(i\phi_{22})$ and $\omega_{22}^{M}\exp(-i\phi_{22})$, respectively. There are no degenerate frequencies associated with this Hamiltonian; that is, the triplet frequencies are $w_{12}=\frac{1}{2}\omega_{22}^{M}$, $w_{13}=-(3\omega_{20}-\omega_{22}^{M})/4$, and $w_{23}=-(3\omega_{20}+\omega_{22}^{M})/4$, while the singlet frequencies are $w_{14}=\omega_{00}-(\omega_{20}-\omega_{22}^{M})/4$, $w_{24}=\omega_{00}-(\omega_{20}+\omega_{22}^{M})/4$, and $w_{34}=\omega_{00}+\frac{1}{2}\omega_{20}$. Making use of these eigenvectors and eigenenergies and Eqs. (A1) and (A5) the nonzero crystal-frame motion functions $g_{00}(t)$ and $g_{20}(t)$ are of the same general form as Eq. (5.1) but with the above frequencies while the $g_{22}(t)$ motion functions are of the form

$$g_{22}(t)=4^{-1}[\cos(w_{23}t)-\cos(w_{12}t)+\cos(w_{14}t)-\cos(w_{24}t)]\exp(-i\phi_{22}) . \tag{5.7}$$

Random hyperfine motion functions are again obtained by averaging these single-particle motion functions over the appropriate distribution functions. The isotropic and cylindrical functions are given by Eq. (5.2) while the planar Gaussian function,

$$\begin{aligned} F_{22}(\omega_{22}^{M},\phi_{22})&=F_{22}(\omega_{22})F_{2\,-2}(\omega_{2\,-2}) \\ &=(2\pi\sigma_{22}^{2})^{-1}\exp\{-(2\sigma_{22}^{2})^{-1}[(\omega_{22}^{M}-\bar{\omega}_{22}^{M})^{2}+4\omega_{22}\bar{\omega}_{22}^{M}\sin^{2}(\tfrac{1}{2}\phi_{22}-\tfrac{1}{2}\bar{\phi}_{22})]\} , \end{aligned} \tag{5.8}$$

is taken to be the product of the two one-dimensional functions with the same spread. With these distribution functions, the isotropic random hyperfine motion function becomes

$$\begin{aligned} 6g_{00}(t)=&\cos(\bar{w}_{12}t)h_{22}^{0}(\tfrac{1}{2}t)-\sin(\bar{w}_{12}t)k_{22}^{0}(\tfrac{1}{2}t)+[\cos(\bar{w}_{13}t)+\cos(\bar{w}_{23}t)]h_{20}(3t/4)h_{22}^{0}(t/4) \\ &-[\sin(\bar{w}_{13}t)+\sin(\bar{w}_{23}t)]h_{20}(3t/4)k_{22}^{0}(t/4)+[\cos(\bar{w}_{14}t)+\cos(\bar{w}_{24}t)]h_{00}(t)h_{20}(t/4)h_{22}^{0}(t/4) \\ &-[\sin(\bar{w}_{14}t)+\sin(\bar{w}_{24}t)]h_{00}(t)h_{20}(t/4)k_{22}^{0}(t/4)+\cos(\bar{w}_{34}t)h_{00}(t)h_{20}(\tfrac{1}{2}t) , \\ h_{22}^{n}(t)=&2\int_{-r}^{\infty}dx\,(x+r)\exp[-x^{2}-2a(x)]I_n(2a(x))\cos(t_{22}x) , \\ k_{22}^{n}(t)=&2\int_{-r}^{\infty}dx\,(x+r)\exp[-x^{2}-2a(x)]I_n(2a(x))\sin(t_{22}x) , \end{aligned} \tag{5.9}$$

where $I_n(x)$ is a modified Bessel function[15] of order n. Here $a(x)$ is $r(x+r)$, where r is the ratio of the average frequency to the spread, $\bar{\omega}_{22}/2^{1/2}\sigma_{22}$. Two special limits of the relaxation functions h and k are of interest, that is, very broad distributions with $r \ll 1$ and very very narrow distributions with $r \gg 1$. For $n=0,1$ these functions reduce to

$$
\begin{aligned}
&h^0_{22}(t)_{r\ll 1} \sim 1-(t_{22})F[\tfrac{1}{2}t_{22}] ,\\
&h^1_{22}(t)_{r\ll 1} \sim (r\pi^{1/2}/4)(1-\tfrac{1}{2}t^2_{22})\exp(-t^2_{22}/4) ,\\
&k^0_{22}(t)_{r\ll 1} \sim \frac{1}{2}t_{22}\exp(-t^2_{22}/4) ,\\
&k^1_{22}(t)_{r\ll 1} \sim (-r/4)\{t_{22}-(2+t^2_{22})F[\tfrac{1}{2}t_{22}]\} ,\\
&h^0_{22}(t) \sim h^1_{22}(t)_{r\gg 1} \sim \exp(-t^2_{22}/4) ,\\
&k^0_{22}(t) \sim k^1_{22}(t)_{r\gg 1} \sim (4r)^{-1}\exp(-t^2_{22}/4) \sim 0 .
\end{aligned}
\tag{5.10}
$$

These relaxation functions involve Dawson's integral,[15]

$$F[x]=\exp(-x^2)\int_0^x dz\exp(z^2) . \tag{5.11}$$

As required very narrow distributions ($r \gg 1$) have only $[\cos(\omega t)]$-type frequency dependence with very long-lived Gaussian relaxation functions. The frequency distributions in this case can be identified with the frequency distributions in their Fourier transform power spectra. Expressions for the remaining crystal and laboratory frame motion functions are given in Appendix B.

VI. LARGE-APPLIED-FIELD RELAXATION FUNCTIONS

When an external field is applied both the frequencies and the amplitudes depend upon the Euler angles. However, when the field is large, the isotropic frequencies will dominate and the full Hamiltonian can be approximated by its diagonal elements alone, that is,

$$
H=(\hbar/4)\begin{bmatrix}
(\omega_{00}+4\omega_{\mathrm{Mu}}-W_{20}) & 0 & 0 & 0\\
0 & (\omega_{00}-4\omega_{\mathrm{Mu}}-W_{20}) & 0 & 0\\
0 & 0 & (\omega_{00}+4\Omega+2C^2W_{20}) & 0\\
0 & 0 & 0 & (-3\omega_{00}-4\Omega+2S^2W_{20})
\end{bmatrix} . \tag{6.1}
$$

Such an approximation is the standard secular high-field approximation[16] of nuclear magnetic resonance. In this approximation the amplitudes are independent of the Euler angles while the frequencies are dependent on them. This dependence is given by Eq. (3.1) which relates the counterframe anisotropic hyperfine frequencies to the crystal-frame frequencies, namely, W_{20} is

$$3(\cos^2\beta-\tfrac{1}{3})\omega_{20}/2+(\tfrac{3}{2})^{1/2}\sin^2\beta[\omega^R_{21}\cos\alpha-\omega^I_{21}\sin\alpha]+(\tfrac{3}{2})^{1/2}\sin^2\beta[\omega^R_{22}\cos 2\alpha-\omega^I_{22}\sin 2\alpha] .$$

Indeed, the triple frequencies are $w_{12}=2\omega_{\mathrm{Mu}}$, $\omega_{13}=\omega_{\mathrm{Mu}}-\Omega-(1+2C^2)W_{20}/4$, and $w_{23}=-[\omega_{\mathrm{Mu}}+\Omega+(1+2C^2)W_{20}/4]$, while the singlet frequencies are $w_{14}=\omega_{00}+\omega_{\mathrm{Mu}}-\Omega-(1+2S^2)\omega_{20}/4$, $w_{24}=\omega_{00}-\omega_{\mathrm{Mu}}+\Omega-(1+2S^2)W_{20}/4$, and $w_{34}=\omega_{00}+2\Omega+(C^2-S^2)W_{20}/2$. The nonzero observable motion functions associated with this Hamiltonian are

$$
\begin{aligned}
&G^C_{\mathrm{L}}(t)=\tfrac{1}{2}[1+\cos^2\lambda+\sin^2\lambda\cos(w_{34}t)] ,\\
&G^{SC}_{\mathrm{CT}}(t)=G^{SS}_{\mathrm{PT}}(t)=\tfrac{1}{2}\cos^2(\tfrac{1}{2}\lambda)[\cos(w_{13}t)+\cos(w_{24}t)]+\tfrac{1}{2}\sin^2(\tfrac{1}{2}\lambda)[\cos(w_{14}t)+\cos(w_{23}t)] ,\\
&G^{SS}_{\mathrm{CT}}(t)=-G^{SC}_{\mathrm{PT}}(t)=\tfrac{1}{2}\cos^2(\tfrac{1}{2}\lambda)[-\sin(w_{13}t)+\sin(w_{24}t)]+\tfrac{1}{2}\sin^2(\tfrac{1}{2}\lambda)[\sin(w_{14}t)-\sin(w_{23}t)] .
\end{aligned}
\tag{6.2}
$$

There is one longitudinal motion function and four transverse motion functions which are grouped in two sets of equivalent pairs that are related by a simple phase. This is, of course, the standard motion of an isotropic muonium atom in an external field with shifted frequencies due to the anisotropic hyperfine components. Assuming Gaussian distributions, the observable longitudinal and transverse random hyperfine motion functions, for a given counter-crystal-frame orientation,

$$
\begin{aligned}
&G^C_{\mathrm{L}}(t)=\tfrac{1}{2}\{1+\cos^2\lambda+\sin^2\lambda\cos(\bar{w}_{34}t)H[(C^2-S^2)t/2]\} ,\\
&G^{SC}_{\mathrm{CT}}(t)=\tfrac{1}{2}[\cos^2(\tfrac{1}{2}\lambda)\cos(\bar{w}_{13}t)+\sin^2(\tfrac{1}{2}\lambda)\cos(\bar{w}_{23}t)]H[(1+2C^2)t/4]\\
&\qquad+\tfrac{1}{2}[\sin^2(\tfrac{1}{2}\lambda)\cos(\bar{w}_{14}t)+\cos^2(\tfrac{1}{2}\lambda)\cos(\bar{w}_{24}t)]h_{00}(t)H[(1+2S^2)t/4] ,\\
&G^{SS}_{\mathrm{PT}}(t)=\tfrac{1}{2}[-\cos^2(\tfrac{1}{2}\lambda)\sin(\bar{w}_{13}t)+\sin^2(\tfrac{1}{2}\lambda)\sin(\bar{w}_{23}t)]H[(1+2C^2)t/4]\\
&\qquad+\tfrac{1}{2}[\sin^2(\tfrac{1}{2}\lambda)\sin(\bar{w}_{14}t)-\cos^2(\tfrac{1}{2}\lambda)\sin(\bar{w}_{24}t)]h_{00}(t)H[(1+2S^2)t/4] ,
\end{aligned}
\tag{6.3}
$$

involve a common relaxation function,

$$H[t]=(2/\pi^{1/2})^5\int_0^\infty dz\, f_{20}(z)\int_0^\infty dx\, f_{21}^R(x)\int_0^\infty dy\, f_{21}^I(y)\int_0^\infty du\, f_{22}^R(u)$$
$$\times\int_0^\infty dv\, f_{22}^I(v)\cos\{\tfrac{1}{2}t_{20}[3z(\cos^2\beta-\tfrac{1}{3})+6^{1/2}s_{21}\sin^2\beta(x\cos\alpha-y\sin\alpha)+6^{1/2}s_{22}\sin^2\beta(u\cos2\alpha-v\sin2\alpha)]\}$$
$$=\exp\{-(3t_{20}^2/16)[3(\cos^2\beta-\tfrac{1}{3})+2s_{21}^2\sin^2 2\beta+2s_{22}^2\sin^4\beta]\}\ , \tag{6.4}$$

where $s_{2m}=\sigma_{2m}/\sigma_{20}$. For a powder sample, where the Euler angles are averaged with equal weights, this common relaxation function becomes

$$H[t]=\int_0^1 dy\exp[-3b(y)t_{20}^2/16]$$
$$b(y)=3(y^2-\tfrac{1}{3})^2+8s_{21}^2y^2(1-y^2)+2s_{22}^2(1-y^2)^2\ . \tag{6.5}$$

Using the method of steepest-descent integrals of this type are found to have the following long-time behavior

$$H[t]_{t\to\infty}\sim[2\pi/3b''(y_0)]^{1/2}(4/t_{20})$$
$$\times\exp[-3b(y_0)t_{20}^2/16]\ . \tag{6.6}$$

If there is only cylindrical distortion, $s_{21}=s_{22}=0$, then the maximum of the integrand occurs at $y_0=3^{-1/2}$ where the function $b(y_0)$ is zero. Thus, for cylindrical anisotropy the relaxation function approaches zero asymptotically as t^{-1}. In contrast, for s_{21} and/or s_{22} nonzero, the function $b(y_0)$ is nonzero so that the resulting relaxation functions approach zero asymptotically as $t^{-1}\exp(-at^2)$. Four types of relaxation functions are depicted in Fig. 1. The pure cylindrical relaxation function is clearly distinguishable from the cases of the cylindrical plus ω_{21}, cylindrical plus ω_{22}, and fully anisotropic relaxation functions. These latter relaxation functions are compared, in Figs. 2, 3, and 4, to Gaussian relaxation functions,

$$\exp[-(t_{20}^2/5)(\tfrac{1}{4}+s_{21}^2+s_{22}^2)]\ ,$$

that have been chosen such that the short-time behaviors are consistent. Although the cylindrical plus ω_{21} and cylindrical plus ω_{22} both differ from the respective Gaussian approximations, it is unlikely that the small deviations will be observable. For the fully anisotropic case the exact function and the exponential approximation to it are indistinguishable.

VII. APPLICATION TO FUSED-QUARTZ DATA

For muonium in bulk silica, the muon-spin polarization may relax only via random anisotropic hyperfine distortions.[17] In an amorphous environment such as bulk fused silica, the hyperfine distortions could only be distributed randomly, both in orientation and magnitude. It is also well known that muonium is static in bulk fused quartz below 50 K.[17,18] Because of these two features, muonium in bulk fused silica provides an excellent test case for the zero- and high-transverse-field random hyperfine spin-relaxation functions developed here. For amorphous samples only the isotropic motion function is observable in zero-field experiments. For example, experiments on powdered silicon dioxide[19] and on fused quartz[17,18] have been performed at TRIUMF. In these experiments static muonium is found on the surfaces of the powder grains or

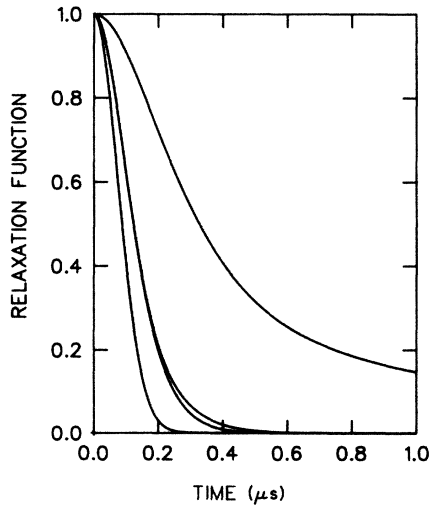

FIG. 1. High-transverse-field relaxation functions for cylindrical, cylindrical plus ω_{21}, cylindrical plus ω_{22}, and fully anisotropic hyperfine tensors. These relaxation functions have, respectively, the slowest to fastest asymptotic approach to zero. The spreads have all been taken to be 10 μs^{-1}, as they are in Figs. 2, 3, and 4.

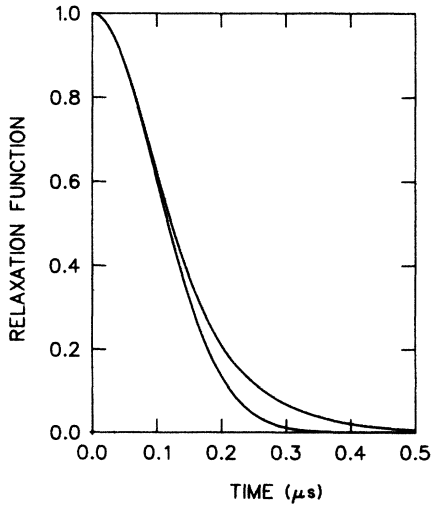

FIG. 2. Comparison of the high-transverse-field relaxation functions for cylindrical plus ω_{21} anisotropies with a Gaussian function which has the same early time behavior. The Gaussian function decays to zero first.

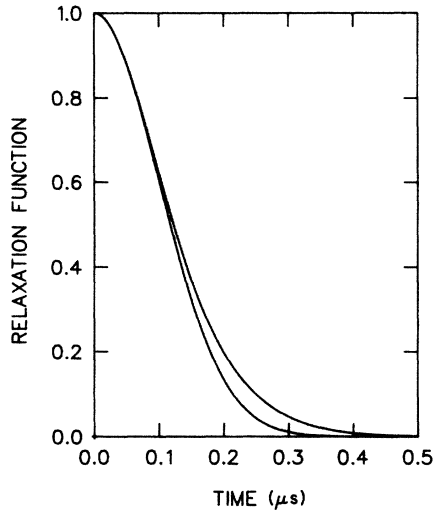

FIG. 3. Comparison of the high-transverse-field relaxation functions for cylindrical plus ω_{22} anisotropies with a Gaussian function which has the same early time behavior. Again, the Gaussian function decays to zero first.

in the bulk fused quartz, while the observed triplet zero-field motion functions of both samples exhibit no average frequencies, decay to zero for long times, and have Lorentzian-type shapes rather than Gaussian. These data can be fit using the random hyperfine distortion theory assuming (i) planar plus cylindrical anisotropies and (ii) Lorentzian-type frequency distributions. The distribution functions are

$$F_{20}(\omega_{20})=(\sigma_{20}/\pi)(\omega_{20}^2+\sigma_{20}^2)^{-1}\,,$$
$$F_{22}(\omega_{22}^M)=(4\omega_{22}^M\sigma_{22}/\pi)(\omega_{22}^{M^2}+\sigma_{22}^2)^{-2}\,, \tag{7.1}$$

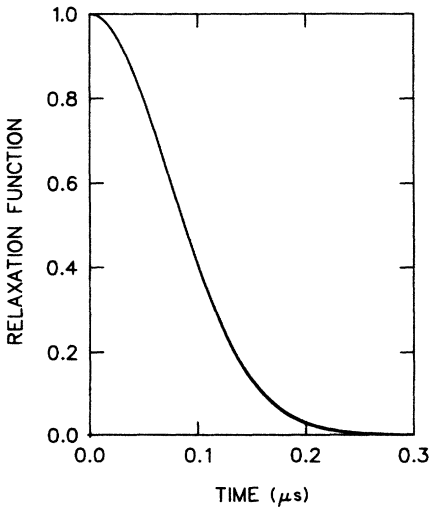

FIG. 4. High-transverse-field relaxation functions for fully anisotropic hyperfine tensors. This relaxation function and the comparable Gaussian function are indistinguishable. Again the spreads are each $10\ \mu s^{-1}$.

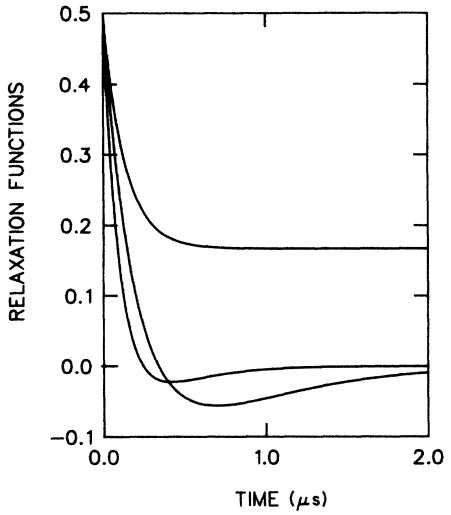

FIG. 5. Lorentzian zero-field isotropic relaxation functions with zero average anisotropic hyperfine frequencies. The relaxation function with the one sixth time tail is that for pure cylindrical anisotropy ($\sigma_{20}=10\ \mu s^{-1}$), while the relaxation function with the longest decay to zero and deepest well is that for pure planar anisotropy ($\sigma_{22}=10\ \mu s^{-1}$). The intermediate relaxation function is an equal mixture of the two ($\sigma_{20}=\sigma_{22}=10\ \mu s^{-1}$).

where $F_{20}(\omega_{20})$ is a one-dimensional Lorentzian and where $F_{22}(\omega_{22}^M)$ is a two-dimensional Lorentzian-type function. This choice of a Lorentzian type, as opposed to a "true" Lorentzian, was made because the former provides a simple analytic expression for the relaxation function that cannot be distinguished experimentally from the latter's relaxation function. Thus, the zero-field relaxation functions are given by the average of $g_{00}(t)$, Eq. (5.1), over these functions, namely,

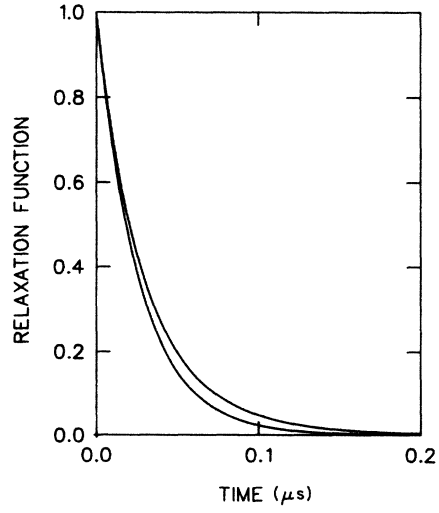

FIG. 6. Comparison of the high-transverse-field relaxation function for cylindrical ($10\ \mu s^{-1}$) plus ω_{22} ($10\ \mu s^{-1}$) anisotropies for a Lorentzian distribution function with an exponential that has the same early time behavior. The exponential decays to zero first.

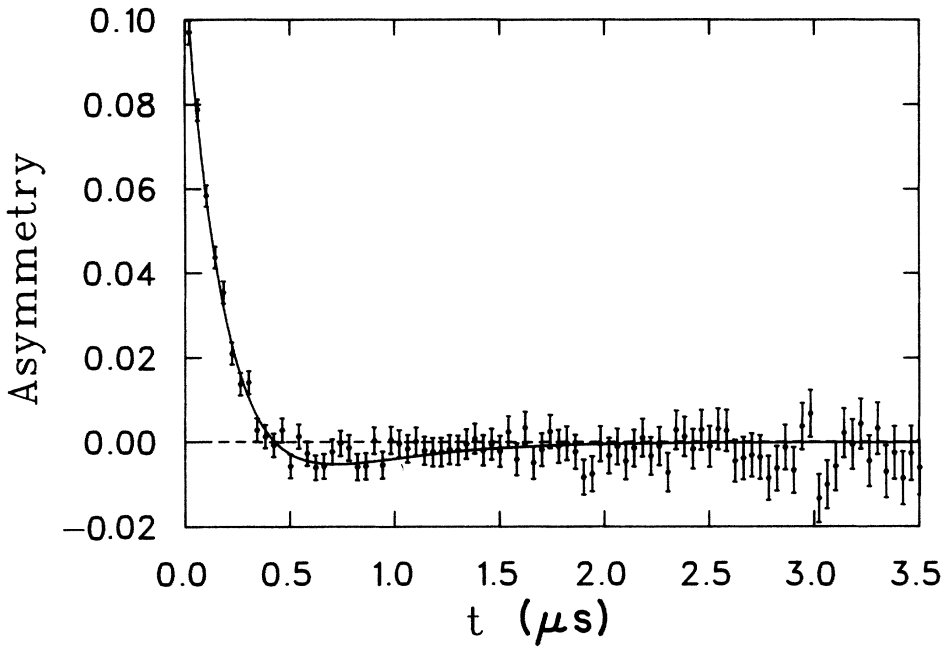

FIG. 7. Fit to the zero-field fused-quartz data[17] at 7 K using the Lorentzian cylindrical plus planar motion function. The values of the half-widths at half-height are $\sigma_{20}=4.7\pm1.3\ \mu s^{-1}$ and $\sigma_{22}=6.2\pm0.5\ \mu s^{-1}$.

$$G_L^C(t)=G_{PT}^{SC}(t)=G_{CT}^{SS}(t)=\tfrac{1}{6}(1-\tfrac{1}{2}t_{22})\exp(-\tfrac{1}{2}t_{22})+\tfrac{1}{3}(1-t_{22}/4)\exp[-(3t_{20}+t_{22})/4]\ , \tag{7.2}$$

where $t_{2M}=\sigma_{2M}t$, see Fig. 5. This is the standard zero-field (ZF) observable relaxation function which can be measured in the longitudinal telescopes and in the transverse telescopes if the skew angles are approximately chosen. The early time dependence of this function, $\frac{1}{2}-m_{ZF}t$, has a slope, m_{ZF}, of $(1+4s_{22}/3)\sigma_{20}/4$. In comparison, using the Lorentzian distributions, the high-transverse-field (7 G) functions, Eqs. (6.3) and (6.4), become

$$\begin{aligned} &G_{CT}^{SC}(t)=\cos(\omega_{Mu}t)\tfrac{1}{2}H[3t/4]\ , \\ &H[t]=(4\pi)^{-1}\int_0^{\pi}d\theta\int_0^{1}dx\exp[-3t_{20}\,|\,(x^2-\tfrac{1}{3})\,|\,/2-(\tfrac{3}{2})^{1/2}t_{22}(1-x^2)\,|\cos\theta\,|\,][1-(\tfrac{3}{2})^{1/2}t_{22}(1-x^2)\,|\cos\theta\,|\,]\ . \end{aligned} \tag{7.3}$$

The early time dependence, $\frac{1}{2}-m_{TF}t$, of $\frac{1}{2}H[3t/4]$ has a slope of $(1+2^{1/2}6s_{22}/\pi)\sigma_{20}/3^{1/2}4$. In Fig. 6 $H[t]$ is compared to a simple exponential, $\exp(-\lambda t)$, with the same early time dependence, that is $\lambda=m_{TF}$. Again, as with the Gaussian functions, these relaxation functions will be very hard to distinguish experimentally. Therefore, the high-transverse-field data are fit to an exponential. As well, the zero-field relaxation functions have a faster loss of polarization for early times than the high-transverse-field (TF) functions, that is, $m_{ZF}>m_{TF}$.

The above choices, Eq. (7.2) and an exponential, are adopted for fitting purposes since they are analytic expressions that contain most of the relevant physics. That is, as with the high-field case, the cylindrical plus ω_{21} and the fully anisotropic hyperfine interactions in zero field have similar motion functions to the cylindrical plus ω_{22}. However, these motion functions cannot be expressed in terms of simple analytic functions. Thus any interpretation of the parameters obtained in a fit with Eq. (7.2) must be considered in light of the above remarks. What can be unambiguously determined is whether more than cylindrical symmetry exists and the relative importance of

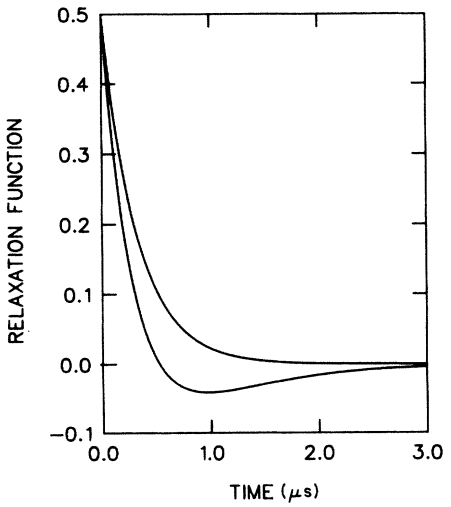

FIG. 8. Comparison of the zero- and high-transverse-field relaxation functions for fused quartz at 7 K. The zero-field relaxation function dips below the origin while the values of the half-widths at half-heights are $\sigma_{20}=4.7\pm1.3\ \mu s^{-1}$ and $\sigma_{22}=6.2\pm0.5\ \mu s^{-1}$.

the noncylindrical components. As well, the fitted parameters in zero field should predict the fitted high-transverse-field relaxation rate to within experimental error. Such a fitting procedure can be performed for low-temperature fused quartz. For example, the zero-field data[17] at 7 K have been fit to Eq. (7.2), see Fig. 7, with half-widths at half-height of $\sigma_{20}=4.7\pm1.3\ \mu s^{-1}$ and $\sigma_{22}=6.2\pm0.5\ \mu s^{-1}$. These values suggest that the initial slope, or relaxation rate, of the high-transverse-field relaxation function should be $m_{TF}=2.9\pm0.6\ \mu s^{-1}$. The actual fitted value,[17,18] $3.4\pm0.5\ \mu s^{-1}$, is, indeed, consistent with this predicted value. Thus the zero- and high-transverse-field relaxation functions predicted by the random hyperfine approximation describe the data to within experimental errors with one set of parameters. The two relaxation functions are compared in Fig. 8.

VIII. CONCLUSION

To conclude, a static relaxation theory describing the time evolution of the muon-spin ensemble polarization, for the case of random hyperfine distortions of the muonium hyperfine interaction, has been developed. Relaxation functions have been calculated for both the zero- and high-field limits. The new zero-field functions, in particular, were shown to have distinctive line shapes and long-time behaviors, exhibiting a strong dependence on the distortion symmetry. This theory was applied to zero- and high-transverse-field data for muonium in fused quartz, by assuming the distortion parameters to be distributed according to Lorentzian-type distributions.

APPENDIX A

Upon use of the isotropic eigenfunctions as basis functions for the expansion of the general eigenfunctions, $|\phi_i\rangle=c_{ik}|k\rangle_0$, of H_{Mu} the counterframe spherical tensor coefficients of the isolated anisotropic muonium-atom spin-spin autocorrelation tensor are

$$
\begin{aligned}
G_{00}(t)&=(12)^{-1}\{|I_{ii}^x|^2+|I_{ii}^y|^2+|I_{ii}^z|^2+2\cos(w_{ij}t)[|I_{ij}^x|^2+|I_{ij}^y|^2+|I_{ij}^z|^2]\}\ ,\\
G_{11}(t)&=-\tfrac{1}{2}\sin(w_{ij}t)\{\mathrm{Im}[I_{ij}^y(I_{ij}^z)^*]-i\,\mathrm{Im}[I_{ij}^x(I_{ij}^z)^*]\}\ ,\\
G_{10}(t)&=-(2)^{-1/2}\sin(w_{ij}t)\mathrm{Im}[I_{ij}^x(I_{ij}^y)^*]\ ,\\
G_{20}(t)&=(\tfrac{2}{3})^{1/2}4^{-1}\{\tfrac{1}{2}[|I_{ii}^x|^2+|I_{ii}^y|^2-|I_{ii}^z|^2]+2\cos(w_{ij}t)(\tfrac{1}{2}[|I_{ij}^x|^2\ |I_{ij}^y|^2]-|I_{ij}^z|^2)\}\\
G_{21}(t)&=4^{-1}[I_{ii}^xI_{ii}^z+iI_{ii}^yI_{ii}^z+2\cos(w_{ij}t)(\mathrm{Re}[I_{ij}^x(I_{ij}^z)^*]+i\,\mathrm{Re}[I_{ij}^y(I_{ij}^z)^*]\}\ ,\\
G_{22}(t)&=-4^{-1}(\tfrac{1}{2}[|I_{ii}^x|^2-|I_{ii}^y|^2]+iI_{ii}^xI_{ii}^y+2\cos(w_{ij}t)\{\tfrac{1}{2}[|I_{ij}^x|^2-|I_{ij}^y|^2]+i\,\mathrm{Re}[I_{ij}^x(I_{ij}^y)^*]\})\ ,
\end{aligned}
\tag{A1}
$$

while the observable longitudinal motion functions become

$$
\begin{aligned}
G_L^C(t)&=\tfrac{1}{4}[|I_{ii}^z|^2+2\cos(w_{ij}t)|I_{ij}^z|^2]\ ,\\
G_L^{SC}(t)&=\tfrac{1}{2}\sin(w_{ij}t)\mathrm{Im}[I_{ij}^x(I_{ij}^z)^*]+\tfrac{1}{4}[I_{ii}^xI_{ii}^z+2\cos(\omega_{ij}t)\mathrm{Re}I_{ij}^x(I_{ij}^z)^*]\ ,\\
G_L^{SS}(t)&=\tfrac{1}{2}\sin(w_{ij}t)\mathrm{Im}[I_{ij}^y(I_{ij}^z)^*]+\tfrac{1}{4}[I_{ii}^yI_{ii}^z+2\cos(w_{ij}t)\mathrm{Re}I_{ij}^y(I_{ij}^z)^*]\ ,
\end{aligned}
\tag{A2}
$$

the observable coplanar transverse motion functions become

$$
\begin{aligned}
G_{CT}^C(t)&=-\tfrac{1}{2}\sin(w_{ij}t)\mathrm{Im}[I_{ij}^x(I_{ij}^z)^*]+\tfrac{1}{4}[I_{ii}^xI_{ii}^z+2\cos(w_{ij}t)\mathrm{Re}I_{ij}^x(I_{ij}^z)^*]\ ,\\
G_{CT}^{SC}(t)&=\tfrac{1}{6}[|I_{ii}^x|^2+3\cos(w_{ij}t)|I_{ij}^x|^2]\ ,\\
G_{CT}^{SS}(t)&=\tfrac{1}{2}\sin(w_{ij}t)\mathrm{Im}[I_{ij}^x(I_{ij}^y)^*]+\tfrac{1}{4}[I_{ii}^xI_{ii}^y+2\cos(w_{ij}t)\mathrm{Re}I_{ij}^x(I_{ij}^y)^*]\ ,
\end{aligned}
\tag{A3}
$$

and the observable perpendicular transverse motion functions become

$$
\begin{aligned}
G_{PT}^C(t)&=-\tfrac{1}{2}\sin(w_{ij}t)\mathrm{Im}[I_{ij}^y(I_{ij}^z)^*]-\tfrac{1}{4}[I_{ii}^yI_{ii}^z+2\cos(w_{ij}t)\mathrm{Re}I_{ij}^y(I_{ij}^z)^*]\ ,\\
G_{PT}^{SC}(t)&=-\tfrac{1}{2}\sin(w_{ij}t)\mathrm{Im}[I_{ij}^x(I_{ij}^y)^*]+\tfrac{1}{4}[I_{ii}^xI_{ii}^y+2\cos(w_{ij}t)\mathrm{Re}I_{ij}^x(I_{ij}^y)^*]\ ,\\
G_{PT}^{SS}(t)&=\tfrac{1}{6}[|I_{ii}^y|^2+3\cos(w_{ij}t)|I_{ij}^y|^2]\ .
\end{aligned}
\tag{A4}
$$

These relaxation functions contain the counterframe components of the muon-spin vector, that is,

$$
\begin{aligned}
I_{ij}^x&=\cos(\tfrac{1}{2}\lambda)[A_{13}^{ij}+A_{24}^{ij}]+\sin(\tfrac{1}{2}\lambda)[A_{23}^{ij}-A_{14}^{ij}]\ ,\\
I_{ij}^y&=i\cos(\tfrac{1}{2}\lambda)[B_{13}^{ij}-B_{24}^{ij}]-\sin(\tfrac{1}{2}\lambda)[B_{14}^{ij}-B_{23}^{ij}]\ ,\\
I_{ij}^z&=C_{12}^{ij}-\cos(\lambda)C_{34}^{ij}+\sin(\lambda)A_{34}^{ij}\ ,
\end{aligned}
\tag{A5}
$$

wherein $A_{kl}^{ij}=c_{ik}^{*}c_{jl}+c_{il}^{*}c_{jk}$, $B_{kl}^{ij}=c_{ik}^{*}c_{jl}-c_{il}^{*}c_{jk}$, and $C_{kl}^{ij}=c_{ik}^{*}c_{jk}-c_{il}^{*}c_{jl}$. The summation in Eqs. (A1)—(A4) over ij is restricted to $i<j$. In general, both the frequencies and the amplitudes are functions of the Euler angles which relate the frames.

APPENDIX B

The remaining nonzero planar plus cylindrical crystal from random hyperfine motion functions,

$$\begin{aligned}
6^{1/2}g_{20}(t)=&\tfrac{1}{2}[\cos(\bar{\omega}_{13}t)+\cos(\bar{\omega}_{23}t)]h_{20}(3t/4)h_{22}^{0}(t/4)\\
&-\tfrac{1}{2}[\sin(\bar{\omega}_{13}t)+\sin(\bar{\omega}_{23}t)]h_{20}(3t/4)k_{22}^{0}(t/4)-\cos(\bar{\omega}_{12}t)h_{22}^{0}(\tfrac{1}{2}t)\\
&+\sin(\bar{\omega}_{12}t)k_{22}^{0}(\tfrac{1}{2}t)+\tfrac{1}{2}[\cos(\bar{\omega}_{14}t)+\cos(\bar{\omega}_{24}t)]h_{00}(t)h_{20}(t/4)h_{22}^{0}(t/4)\\
&-\tfrac{1}{2}[\sin(\bar{\omega}_{14}t)+\sin(\bar{\omega}_{24}t)]h_{00}(t)h_{20}(t/4)k_{22}^{0}(t/4)-\cos(\bar{\omega}_{34}t)h_{00}(t)h_{20}(\tfrac{1}{2}t)\ ,\\
4g_{22}(t)=&-[\cos(\bar{\omega}_{13}t)-\cos(\bar{\omega}_{23}t)]h_{20}(3t/4)h_{22}^{1}(t/4)\exp(-i\bar{\phi}_{22})\\
&+[\sin(\bar{\omega}_{13}t)-\sin(\bar{\omega}_{23}t)]h_{20}(3t/4)k_{22}^{1}(t/4)\exp(-i\bar{\phi}_{22})\\
&+[\cos(\bar{\omega}_{14}t)-\cos(\bar{\omega}_{24}t)]h_{00}(t)h_{20}(t/4)h_{22}^{1}(t/4)\exp(-i\bar{\phi}_{22})\\
&-[\sin(\bar{\omega}_{14}t)-\sin(\bar{\omega}_{24}t)]h_{00}(t)h_{20}(t/4)k_{22}^{1}(t/4)\exp(-i\bar{\phi}_{22})\ ,
\end{aligned}\tag{B1}$$

are observable if experiments are performed on single crystals. In particular, when the counter and crystal frames are synonymous, the observable longitudinal motion functions are given by

$$\begin{aligned}
&G_{\mathrm{L}}^{C}(t)=\tfrac{1}{2}[\cos(\bar{\omega}_{12}t)h_{22}^{0}(\tfrac{1}{2}t)-\sin(\bar{\omega}_{12}t)k_{22}^{0}(\tfrac{1}{2}t)]+\tfrac{1}{2}\cos(\bar{\omega}_{34}t)h_{00}(t)h_{20}(\tfrac{1}{2}t)\ ,\\
&G_{\mathrm{L}}^{SC}(t)=G_{\mathrm{L}}^{SS}(t)=0\ ,
\end{aligned}\tag{B2}$$

the observable coplanar transverse motion functions are given by

$$\begin{aligned}
&G_{\mathrm{CT}}^{C}(t)=0\ ,\\
&G_{\mathrm{CT}}^{SC}(t)=4^{-1}[\cos(\bar{\omega}_{13}t)h_{m}(t/4)-\sin(\bar{\omega}_{13}t)k_{m}(t/4)]h_{20}(3t/4)+4^{-1}[\cos(\bar{\omega}_{23}t)h_{p}(t/4)-\sin(\bar{\omega}_{23}t)k_{p}(t/4)]h_{20}(3t/4)\\
&\quad+4^{-1}[\cos(\bar{\omega}_{14}t)h_{p}(t/4)+\sin(\bar{\omega}_{14}t)k_{p}(t/4)]h_{00}(t)h_{20}(t/4)\\
&\quad+4^{-1}[\cos(\bar{\omega}_{24}t)h_{m}(t/4)-\sin(\bar{\omega}_{24}t)k_{m}(t/4)]h_{00}(t)h_{20}(t/4)\ ,
\end{aligned}\tag{B3}$$

$$\begin{aligned}
G_{\mathrm{CT}}^{SS}(t)=&\,4^{-1}[\cos(\bar{\omega}_{13}t)-\cos(\bar{\omega}_{23}t)]\sin\bar{\phi}_{22}h_{20}(3t/4)h_{22}^{1}(t/4)-4^{-1}[\sin(\bar{\omega}_{13}t)-\sin(\bar{\omega}_{23}t)]\sin\bar{\phi}_{22}h_{20}(3t/4)k_{22}^{1}(t/4)\\
&+4^{-1}[\cos(\bar{\omega}_{14}t)+\cos(\bar{\omega}_{24}t)]\sin\bar{\phi}_{22}h_{00}(t)h_{20}(t/4)h_{22}^{1}(t/4)\\
&-4^{-1}[\sin(\bar{\omega}_{14}t)-\sin(\bar{\omega}_{24}t)]\sin\bar{\phi}_{22}h_{00}(t)h_{20}(t/4)k_{22}^{1}(t/4)\ ,
\end{aligned}$$

and the observable perpendicular transverse motion functions are given by

$$\begin{aligned}
&G_{\mathrm{PT}}^{C}(t)=0,\quad G_{\mathrm{PT}}^{SC}(t)=G_{\mathrm{PT}}^{SS}(t)\ ,\\
&G_{\mathrm{PT}}^{SS}(t)=4^{-1}[\cos(\bar{\omega}_{13}t)h_{p}(t/4)-\sin(\bar{\omega}_{13}t)k_{p}(t/4)]h_{20}(3t/4)\\
&\quad+4^{-1}[\cos(\bar{\omega}_{23}t)h_{m}(t/4)-\sin(\bar{\omega}_{23}t)k_{m}(t/4)]h_{20}(3t/4)\\
&\quad+4^{-1}[\cos(\bar{\omega}_{14}t)h_{p}(t/4)-\sin(\bar{\omega}_{14}t)k_{p}(t/4)]h_{00}(t)h_{20}(t/4)\\
&\quad+4^{-1}[\cos(\bar{\omega}_{24}t)h_{m}(t/4)-\sin(\bar{\omega}_{24}t)k_{m}(t/4)]h_{00}(t)h_{20}(t/4)\ ,
\end{aligned}\tag{B4}$$

where

$$b_{p\text{ or }m}(t)=b_{20}^{0}(t)\pm\cos\bar{\phi}_{22}b_{22}^{1}(t),\quad b=h,k\ .\tag{B5}$$

---

*Present address: AT&T Bell Labs, 600 Mountain Avenue, Murray Hill, NJ 07974.

[1]Proceedings of the First International Topical Meeting on Muon Spin Rotation, edited by F. N. Gygax, W. Kundig, and P. F. Meier [Hyperfine Interac. 6, (1979)].

[2]Proceedings of the Second International Topical Meeting on Muon Spin Rotation, edited by J. H. Brewer and P. W. Percival [Hyperfine Interact. 8, (1981)].

[3]Proceedings of the Yamada Conference VII, Muon Spin Rotation and Associated Problems, edited by T. Yamazaki and K.

Nagamine [Hyperfine Interact. **17-19**, (1984)].
[4]D. G. Fleming, D. M. Garner, L. C. Vaz, D. C. Walker, J. H. Brewer, and K. M. Crowe, Adv. Chem. **175**, 279 (1979).
[5]A. Schenck, in *Nuclear and Particle Physics at Intermediate Energies,* edited by J. B. Warren (Plenum, New York, 1976), p. 159.
[6]See, for example, G. Arfken, *Mathematical Methods for Physicists* (Academic, New York, 1970).
[7]R. E. Turner, Phys. Rev. B **31**, 112 (1985).
[8]R. E. Turner, Hyperfine Interact. **23**, 237 (1985).
[9]J. H. Brewer, Hyperfine Interact. **8**, 831 (1981).
[10]J. L. Beveridge, J. Doornbos, D. M. Garner, D. J. Arseneau, I. D. Reid, and M. Senba, Nucl. Instrum. Methods A **240**, 316 (1985).
[11]F. M. Chen, H. Moraal, and R. F. Snider, J. Chem. Phys. **57**, 542 (1972).
[12]L. W. Hunter and R. F. Snider, J. Chem. Phys. **61**, 1151 (1974).
[13]See, for example, A. Messiah, *Quantum Mechanics* (Wiley, New York, 1958), Vol. 2.
[14]G. Baym, *Lectures on Quantum Mechanics* (Benjamin-Cummings, Reading, Mass., 1969).
[15]M. Abramowitz and I. A. Stegun, *Handbook of Mathematical Functions* (Dover, New York, 1964).
[16]See, for example, A. Abragam, *Principles of Nuclear Magnetism* (Clarendon, Oxford, England, 1970).
[17]J. H. Brewer, Hyperfine Interact. **8**, 375 (1981).
[18]D. P. Spencer, Ph.D. thesis, University of British Columbia, 1985 (unpublished).
[19]D. R. Harsham, Ph.D. thesis, University of British Columbia, 1986 (unpublished).